Numerical simulations of a thermocline in a pressure-driven flow between two infinite horizontal plates

Robert Moestam[a)]
Department of Electromagnetics, Chalmers University of Technology, SE-41296 Göteborg, Sweden

Lars Davidson[b)]
Department of Thermo and Fluid Dynamics, Chalmers University of Technology, SE-41296 Göteborg, Sweden

(Received 22 February 2005; accepted 14 March 2005; published online 13 July 2005)

Direct numerical simulations of pressure-driven flow between two infinite horizontal plates with a stabilizing temperature difference imposed on the plates are presented, for different Grashof numbers. A thermocline-like solution is obtained. The thermocline decorrelates velocity fluctuations which results in a high mean flow velocity. Temperature fluctuations decorrelate from the vertical velocity fluctuations and it is found that although $\langle T'^2 \rangle$ and $\langle v'^2 \rangle$ increase with Grashof number, $\langle v'T' \rangle$ decreases. It is argued from the simulations that this behavior is due to internal gravity waves. It is also found that the demands on the size of the computational box increase with Grashof number. © *2005 American Institute of Physics*. [DOI: 10.1063/1.1920648]

I. INTRODUCTION

The transport of heat in turbulent flows is difficult to analyze owing to its nonlinear nature. Only a few analytical solutions for special cases are known. Numerical simulations are thus a useful tool for examining different physical aspects of Navier–Stokes equations. The wide range of time scales and length scales makes it extremely costly to compute all scales of turbulence. The advancement of computer power has made it possible to make direct numerical simulations (DNSs) of all turbulent scales in simple geometries and low Reynolds numbers.

DNS has been successful in calculating the behavior of turbulent flow as well as transition flow.[1] It is so far our only tool to investigate the underlying physics of turbulence using theoretical first-principle basis. Understanding the physical properties of the flow can guide in the construction of turbulence models needed for engineering purposes. DNS also gives excellent reference solutions when evaluating turbulence models.

Transport barriers are zones in which the turbulent fluctuations are reduced, thus resulting in a decrease in turbulent transport. These are naturally occurring phenomena, known in fluid mechanics as inversions and thermoclines, caused mainly by stabilizing gradients, as reviewed in Ref. 2. Transport barriers can occur whenever there are competing sources of free energy to the turbulence. The phenomena have also recently been recognized in fusion plasma experiments.[3] Transport barriers in fusion plasmas are, however, due to different mechanisms than the process studied here.[4]

Understanding transport barriers is of major importance in attempts to control turbulence. It can provide a means for reducing the drag coefficient or reducing transport in order to improve thermal insulation. It can also contribute to enhance the predictability of the turbulence models used extensively in industry today. In fusion plasma, knowledge of how to control turbulence may greatly improve the confinement properties of a plasma, providing a possibility to enhance the efficiency and reduce the size of future fusion reactors.

Properties of pressure-driven channel flow are well known and reasonably simple to simulate. It also serves as an excellent test bench for turbulence models. In this context less examined branches of the problem are transport barriers and relaminarization, where inverse cascade dynamics and wave motion may be of importance to heat transfer. However, the physics of wall turbulence-wave motion interaction is poorly understood and is outside the scope of the present study. In stratified flow the turbulence was shown to decompose into internal wave motion and two-dimensional turbulence[5] and as shown by Kraichnan,[6] the energy cascades from small to large scales, known as inverse cascade, in two-dimensional Euler equations. Inertial wave dynamics has been extensively studied in context of atmospheric physics, both experimentally and numerically, see Refs. 7 and 8 and references therein. The effect of two dimensionality and wave motion is not accounted for in the standard turbulence models but may show to be important for studying heat and particle transports.

For pressure-driven flow between two infinite horizontal plates with stabilizing temperature boundary conditions, the flow in the core can be turbulent even though the local Richardson number is above the critical value for stability. This was found by Iida and Kasagi,[9] in work with direct numerical simulations. The flow formed a thermocline in the core of the channel and eventually underwent a transition to one-sided turbulence as Grashof number increased. Studies of the turbulent structure showed that the main turbulent structure is internal gravity waves. Garg, Ferziger, Monismith, and Koseff[10] showed with LES (large eddy simulation) that a transition of the relaminarized part of the channel can be

[a)]Electronic mail: robert.moestam@fsdynamics.se
[b)]Electronic mail: lada@chalmers.se

triggered by the turbulent part such that the flow becomes turbulent in the full channel. This indicates that one-sided turbulence can have an intermittent nature.

For this study, we choose pressure-driven channel flow to investigate how a stabilizing temperature affects the flow and thereby allowing a possibility for a transport barrier to develop in the presence of wall shear flow. Due to the long time scales involved in obtaining statistically steady-state turbulence, the relaminarization process is outside the scope of the article, but some properties of relaminarization due to a small box size are discussed, in connection to the results obtained by Garg, Ferziger, Monismith, and Koseff[10] and Iida and Kasagi.[9]

The paper is organized as follows. In Sec. II we outline the model and numerical setup of the calculations. In Sec. III we present the results from the computations. In Sec. IV we discuss the effects of box size and resolution and integration time in connection to Garg, Ferziger, Monismith, and Koseff[10] and Iida and Kasagi.[9] Section V contains a strong argument based on the simulation results that the dominant turbulent structure is internal gravity waves. Section VI concludes the paper and summarizes the findings.

II. MODEL EQUATIONS AND NUMERICS

We use a research code, developed at the Department of Thermo and Fluid Dynamics at Chalmers University of Technology, intended to solve incompressible Navier–Stokes (NS) equation. The incompressible NS equations are solved in a pressure-driven flow between two infinite horizontal plates with stabilizing temperature boundary conditions. The temperature effect on the momentum equations is included by the Boussinesq approximation. Dirichlet (i.e., no slip for the momentum equation and $T=\pm 1$ for temperature equation) boundary conditions were imposed on the walls and periodic boundary conditions were used in the spanwise and streamwise directions. The Reynolds number was set to 180 on the basis of wall units. The incompressible Navier–Stokes and thermal energy equations are

$$\frac{\partial u_i}{\partial t}+\frac{\partial}{\partial x_j}(u_i u_j)=\delta_{i1}-\frac{1}{\rho}\frac{\partial p}{\partial x_i}+\frac{1}{\mathrm{Re}}\frac{\partial^2 u_i}{\partial x_j\,\partial x_j}+\frac{\mathrm{Gr}}{\mathrm{Re}^2}T\delta_{i2},\quad \frac{\partial u_i}{\partial x_i}=0, \tag{1}$$

$$\frac{\partial T}{\partial t}+\frac{\partial u_j T}{\partial x_j}=\frac{1}{\mathrm{RePr}}\frac{\partial}{\partial x_j}\frac{\partial T}{\partial x_j}, \tag{2}$$

$$\mathrm{Gr}=\frac{g\beta(T_t-T_0)L^3}{\nu^2},\quad \mathrm{Re}=\frac{u^* L}{\nu}, \tag{3}$$

where $\mathrm{Pr}=0.72$, L is half the channel height ($L=1$), subscript t denotes the top wall, T_0 denotes the reference temperature ($T_0=0$), u_* is the friction velocity ($u_*=1$), and ν is the viscosity.

The equations are discretized using second-order central differencing in space and Crank–Nicolson in time. The equation system is solved by employing an implicit, two-step time advancement method.[11] The momentum equations are solved using a symmetric Gauss–Seidel solver, and Poisson equation for the pressure is solved employing an efficient multigrid method.[12] The code has been validated against other DNS (Ref. 13) codes in the nonbuoyancy case.

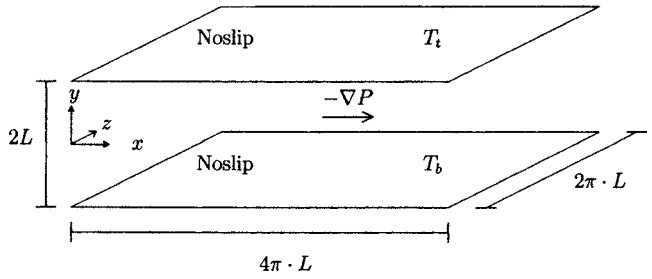

FIG. 1. Geometry of the computational domain. y direction is referred to as vertical, x as streamwise, and z as spanwise.

The dimensions of the computational box were $4\pi L$ in the streamwise direction (x direction), $2\pi L$ in the spanwise direction (z direction), and $2L$ in the vertical direction (y direction), see Fig. 1. The grid was $66\times 66\times 130$, with uniform spacing in the spanwise and streamwise directions, and the vertical spacing was increased by 1.08 towards the middle of the channel, producing a higher resolution at the walls. This gives a smallest gridspacing at the wall of $0.003725L$, i.e., $0.67y^+$ and a largest in the center of $0.008097L$, i.e., $15y^+$. The gridspacing in the streamwise and spanwise directions are $\Delta x^+=35$ and $\Delta z^+=9$, respectively. The largest Courant–Friedricks–Lewey (CFL) number was about 0.7.

III. RESULTS

Initial conditions were taken from nonbuoyant turbulence simulations since the simulations are subcritical, i.e., perturbations of an initial state do not survive unless they are of finite size and the time to reach fully developed turbulence is substantially reduced by taking the initial conditions from previous simulations. The simulations were run until there were no visible trends of the time evolution of the wall shear stress and the total shear stress profile varied as $-1+y/L$. The time to reach fully developed turbulence is not studied in detail in this article but a strong increase of the time before reaching a fully developed turbulence with Grashof number is noticed and discussed later. The plots presented are space and time averaged over the nodes in the spanwise and streamwise directions for 5000 time steps, denoted by $\langle\cdot\rangle$. The sampling frequency varied with Grashof number between 2.5×10^{-3} and 4.9×10^{-3} as the time step of the simulations changed, due to the variation of the velocity with Grashof numbers.

As visible in Fig. 2(a) the influence of buoyancy on the flow becomes stronger with Grashof number and the turbulent state of the flow changes. The bulk streamwise velocity $\langle u\rangle$ increases with Grashof number, due to the decrease of the turbulent shear stress, Fig. 2(e). As Grashof number increases the mean velocity profile peaks towards the middle of the channel.

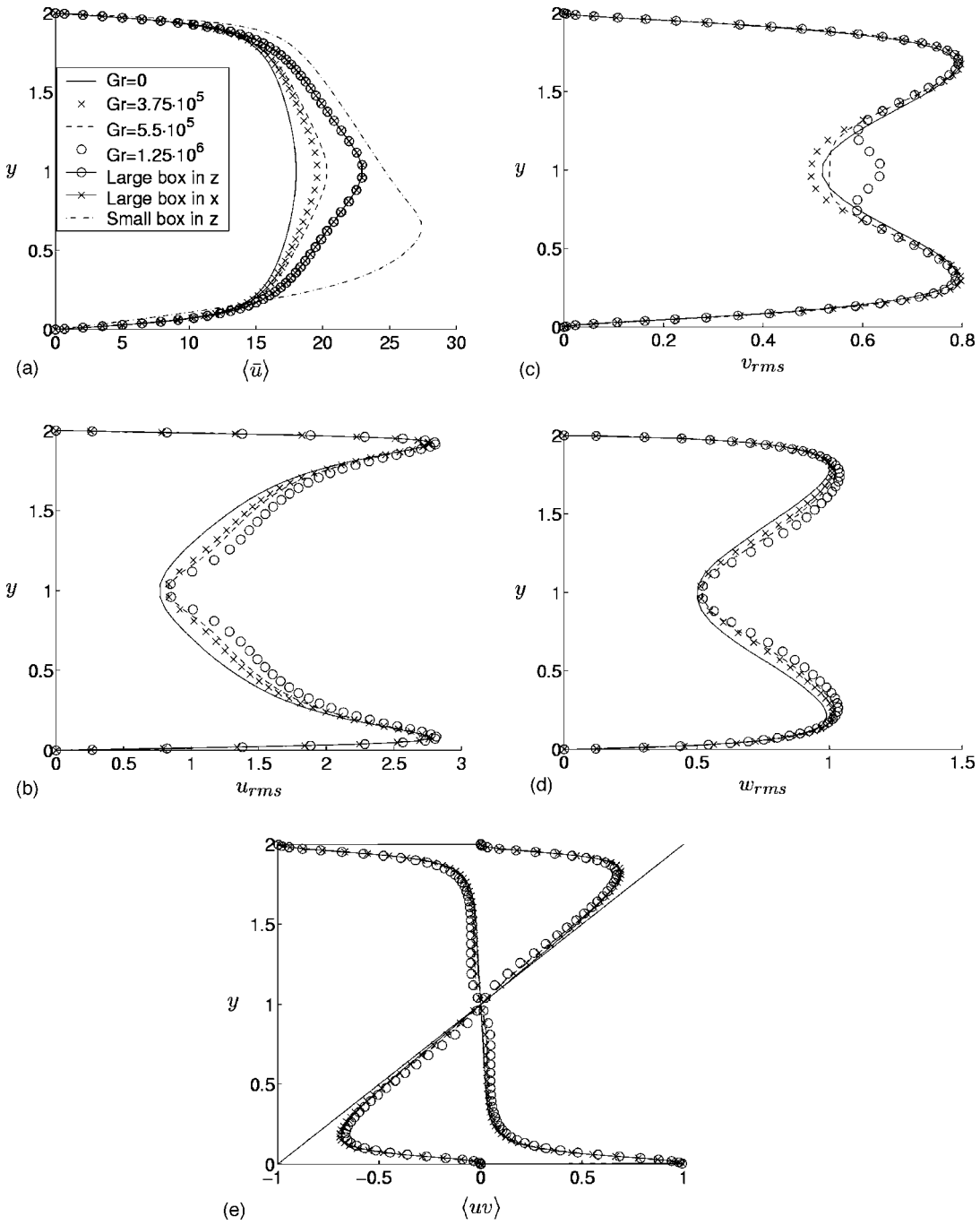

FIG. 2. Mean quantities of the velocity field. (a) Mean streamwise velocity profile. (b) Rms of streamwise velocity fluctuations profile. (c) Rms of vertical velocity fluctuation profile. (d) Rms of spanwise velocity fluctuations profile. (e) Profile of turbulent shear stress $\langle uv \rangle$. The straight solid line is the total stress. The lines starting at $y=2, \langle uv \rangle = -1$ are the negative viscous shear stress, i.e., $-1/Re \cdot \partial U/\partial y$.

The peak of the streamwise velocity is caused by a decorrelation of the vertical and streamwise velocity fluctuations. The increased shear of the mean velocity leads to an increased turbulent production resulting in higher level of turbulence, Fig. 3, for the major part of the channel. The rms of streamwise velocity fluctuations, Fig. 2(b), shows similar behavior and shows a significant effect of damping by buoyancy in the middle of the channel, which lowers the fluctuation level. For the spanwise velocity fluctuations the effect is smaller and a damping is seen, Fig. 2(d). The largest effect is on the vertical velocity fluctuations, Fig. 2(c), which are damped with increasing Grashof number, with exception for in the region $0.75 < y < 1.25$, where it increases due to an increased pressure gradient velocity term, see Fig. 4.

The mean temperature profile, Fig. 5(a), shows a clear deviation from the nonbuoyant case. The temperature profile flattens in the middle of the channel which is the same as saying that the temperature gradient is large there. The heat transport over the x-z plane has to be independent of height and since the turbulent transport of temperature is reduced in the middle, see Fig. 5(b), the viscous diffusive heat has to increase resulting in a higher-temperature gradient.

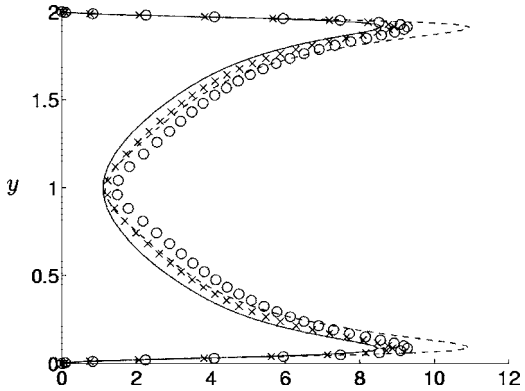

FIG. 3. Turbulent kinetic energy. For legend see Fig. 2(a).

A feedback loop makes the buoyancy effect strong in the middle of the channel. At the walls the shear production is too large for the buoyancy to affect the turbulence, see Figs. 6(a) and 6(b). In the center where the turbulence production is low the buoyancy sink is competitive with the turbulence production. In the middle of the channel the buoyancy effect, due to the temperature gradient, decreases the turbulent heat transport. To keep the total heat transport constant with respect to height, the mean temperature gradient must increase. The increased temperature gradient makes the buoyancy effect stronger and damps the turbulent heat transport even more and the feedback loop is closed.

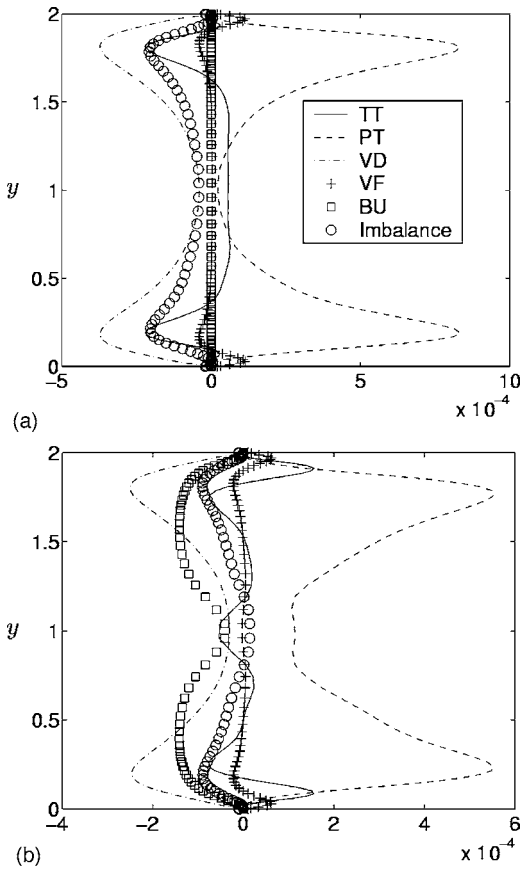

FIG. 4. Balances of $\langle v'^2 \rangle$. The terms are defined by Eq. (A4). (a) Gr=0. (b) $\mathrm{Gr}=1.25\cdot 10^6$.

In the middle of the channel both v_{rms} and T_{rms}, Figs. 2(c) and 5(d) increase with increasing Grashof number, whereas the magnitude of the turbulent heat transport $\langle v'T' \rangle$, Fig. 5(b), decreases. The buoyancy increases the level of fluctuations but does so in an ordered fashion such as to decorrelate the variables. This is an indication that internal gravity waves may have been excited, with a phase of $\pi/2$ between v and T. Internal gravity waves are linear waves due to the restoring force of the stabilizing temperature gradient (for details see Ref. 14).

In the middle of the channel the pressure gradient $\partial\langle p \rangle/\partial y$ and the buoyancy term in the vertical momentum equation are in balance. As the buoyancy term increases with Grashof number the pressure gradient increases and it is reasonable to assume that also the fluctuating pressure gradient increases leading to an increase in the pressure gradient-velocity term in Eq. (A2). This, together with the fact that the magnitude of the buoyancy term $\mathrm{Gr}\langle v'T' \rangle/\mathrm{Re}^2$ decreases, explains why $\langle v'^2 \rangle$ increases for increasing Grashof number.

The balance for $\langle T'^2 \rangle$ is not explicitly dependent on buoyancy and is only implicitly affected by the buoyancy due to the change of vertical velocity fluctuations and the change in temperature gradient. The main reason for the increase of $\langle T'^2 \rangle$ in the middle seems to be due to a decreased dissipation. The decrease in dissipation can be explained by that the turbulence exhibits structures of larger scales. From Figs. 7(a) and 7(b) we see that the correlation length has indeed increased in the middle of the channel. The increase of length scales may be due to the inverse cascade dominating two-dimensional turbulence.[6] The relevance of two dimensionality and thereby the inverse cascade is expected to increase as the flow stratifies, and decouples the dynamics of the x-z planes.

IV. BOX SIZE AND RESOLUTION

The box size and resolution are of vital importance when simulating these flows. To address this issue calculations were made in a box of dimensions $2\pi L \times 2L \times 0.5L\pi$ with a $66\times 66\times 66$ grid. For Gr=0 the results on that grid were in very good agreement with the simulations presented. For $\mathrm{Gr}=1.25\times 10^6$ the situation was worse. A decrease in the streamwise box size did not show a significant difference, but a decrease of box size in the spanwise direction changed the flow significantly. Using the box size $4\pi L \times 2L \times \pi L$ and a $66\times 66\times 66$ grid for $\mathrm{Gr}=1.25\times 10^6$ the symmetry of the flow around $y=1$ was broken and one-sided turbulence developed, see Fig. 2(a) (curve labeled small box in z). The qualitative features of flow were then very similar to what was observed at higher Gr number in Ref. 9. The high demands on the computational domain as well as on the resolution stop us from investigating higher Gr numbers for this article. Computations with a box of $4\pi L\times 2L\times 2\pi L$ and a $66\times 66\times 66$ grid showed significant change for both Gr=0 and $\mathrm{Gr}=1.25\times 10^6$. This shows that for higher Grashof numbers it is necessary to increase the box size in the spanwise direction while maintaining the resolution of the small scales in that direction. This together with the correlation functions Figs. 7(a) and 7(b) make us conclude that the turbulent struc-

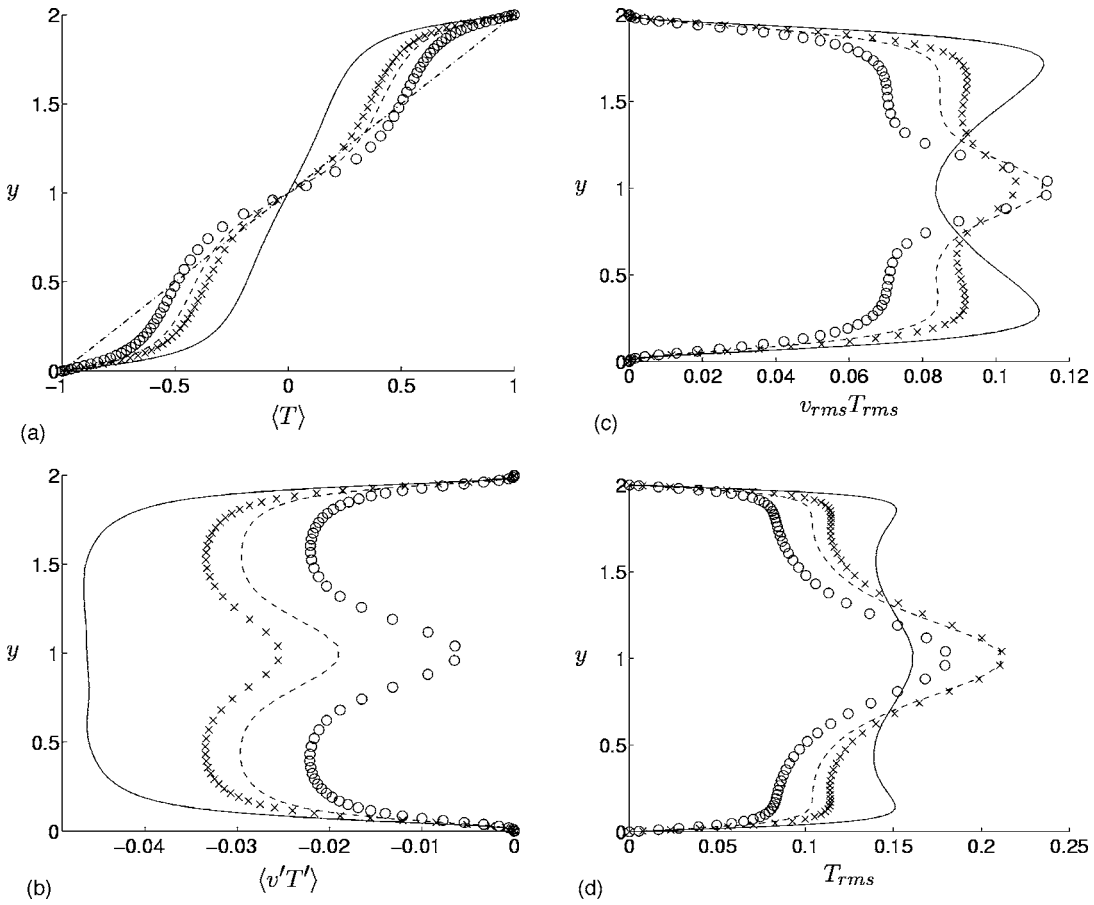

FIG. 5. Mean quantities of the thermal field and coupling to the vertical velocity field. For the legend, see Fig. 2(a). (a) Mean temperature profile. (b) Profile of turbulent heat transport, $\langle v'T' \rangle$. (c) Profile of the product of vertical and temperature fluctuations $v_{\mathrm{rms}}T_{\mathrm{rms}}$. (d) Profile of temperature fluctuations T_{rms}.

tures become larger with Gr, thus demanding larger computational boxes. Simulations using the same gridspacing but 1.5 times longer in spanwise ($3\pi L$) and streamwise ($6\pi L$) directions, respectively, Fig. 2(a), show that the box is sufficiently large.

The $\mathrm{Gr}=1.25\times10^6$ simulations presented in this paper showed similar behavior to that of the transient simulations of Garg, Ferziger, Monismith, and Koseff.[10] They observed that the flow relaminarizes in half of the channel and then undergoes transition and changes sides of turbulent and relaminarized parts of the flow. In our case the flow eventually became symmetric again after long integration time, i.e., approximately 50 000 time steps, which corresponds to about 400 flow through times. The transient simulations of Garg, Ferziger, Monismith and Koseff are therefore likely to become symmetric and develop steady-state turbulence if long enough integration times were to be used. Note that for the simulations with small computational box in the z direction the flow was relaminarized in half of the channel and showed no sign of changing sign, even for long integration times.

V. INTERNAL GRAVITY WAVES

Looking at the time evolution of the wall shear stress, Fig. 8(a), for $\mathrm{Gr}=1.25\times10^6$ one notices a pronounced periodicity. Linearizing Eqs. (1) and (2) around mean temperature T_0 and velocity U_0 profiles and Fourier decomposing the perturbation in time and space give the dispersion relation for the linear wave structure, for details see Ref. 15,

$$(\omega - U_0 k_x)^2 (k_x^2 + k_y^2 + k_z^2) = (k_x^2 + k_y^2)\left[N^2 - i\frac{\partial U_0}{\partial y}(\omega - U_0 k_x)\right], \tag{4}$$

where ω is the complex angular frequency, $\mathbf{k}=(k_x,k_y,k_z)$ the wave-number vector and $N=\sqrt{\mathrm{Gr}/\mathrm{Re}^2 dT_0/dy}$ is the Brunt–Väisälä frequency. We see that the mean velocity gives a Doppler shift. Neglecting the Doppler shift and assuming that the influence of mean velocity shear is small on the linear wave structure give the dispersion relation for internal gravity waves[14]

$$\omega^2 = N^2 \frac{k_x^2 + k_z^2}{k_x^2 + k_y^2 + k_z^2} = N^2 \frac{\dfrac{1}{L_x^2} + \dfrac{1}{L_z^2}}{\dfrac{1}{L_x^2} + \dfrac{1}{L_y^2} + \dfrac{1}{L_z^2}}, \tag{5}$$

where L_x, L_y, and L_z are the length scales of the wave. Close to the wall shear produced turbulence determine the turbulent structure, whereas in the middle the buoyancy effect is the most prominent. With this in mind we estimate the height of the wave to be one third of channel height, i.e., $L_y = 0.66L$ and assuming that the wave structure is of the order

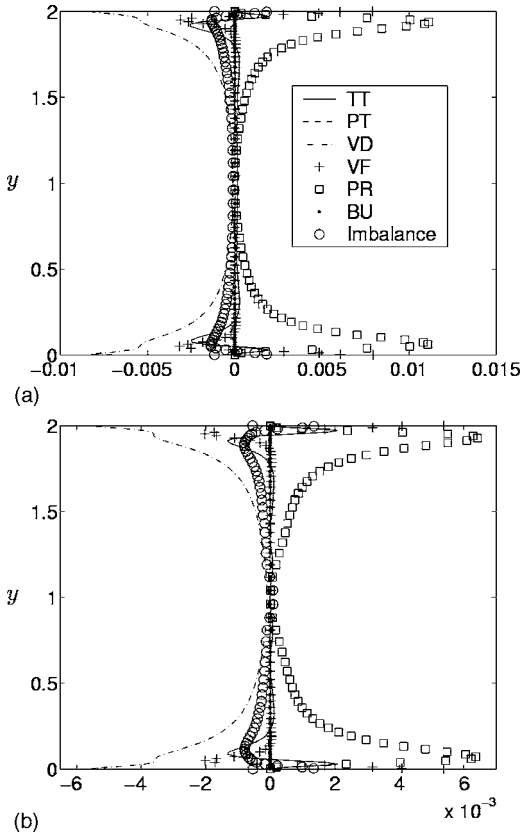

FIG. 6. Kinetic-energy balance. The terms are defined by Eq. (A1). (a) Gr=0. (b) Gr=$1.25\cdot10^6$.

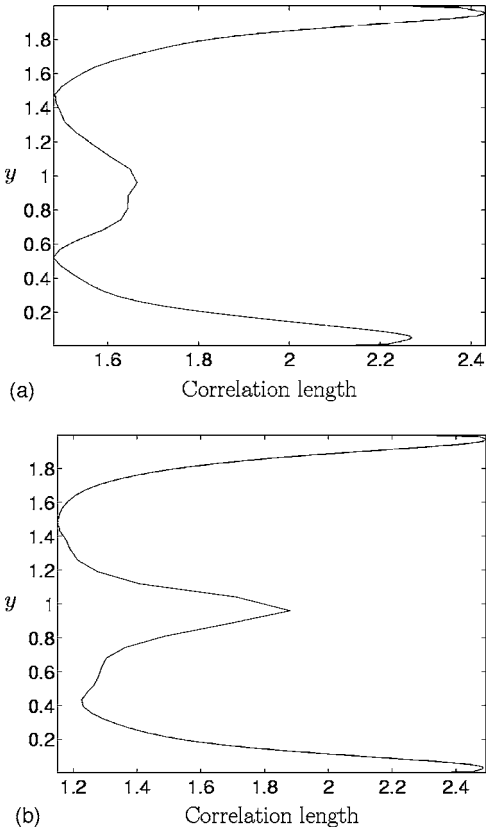

FIG. 7. Correlation length (integral length scale), $\int\int f(x)f(x-x')dx'dx/\int f(x)^2dx$, of streamwise velocity fluctuations in the streamwise direction. (a) Gr=0. (b) Gr=$1.25\cdot10^6$.

of the box size in the other directions, i.e., $L_x=4\pi L$, $L_z=2\pi L$ gives a period time of $\mathcal{T}\approx 8.7$ time units. The temperature gradient was estimated with its laminar profile ($d\langle T\rangle/dy=1$), since this is close to the profile in the middle of the channel. The Brunt–Väisälä frequency is the highest frequency of internal gravity waves and in this case corresponds to a period time of $\mathcal{T}=1.0$, corresponding to infinite wavelength in the y direction. The peak in the power spectral density of the wall shear stress in Fig. 8(b) corresponds to a period time of 6.7. This estimation shows that it is likely that the periodicity of the wall shear stress is caused by spatially extended internal gravity waves. It also implies that internal gravity waves affect the turbulent structure near the walls.

During the box size convergence studies it was noted that the magnitude of the peak was increased when increasing the box size in the streamwise direction and decreased for an increased box size in the spanwise direction. The frequency for the peak turned out to be constant. That the peak is decreased when extending the box in the spanwise direction can be due to the fact that the friction force studied is then integrated over a larger area. We have, however, no explanation on why the peak increases with an increased box size in the streamwise direction.

VI. CONCLUSIONS AND FUTURE CALCULATIONS

Calculations are presented of turbulent pressure-driven channel flow for which stabilizing temperature boundary conditions were imposed. A thermocline-like solution is obtained.

It is found that buoyancy increases the vertical velocity fluctuations as well as the temperature fluctuations and at the same time decorrelate the variables. The same goes for u' and v'. It is likely that internal gravity waves are excited, which causes this behavior.

The importance of the box size and resolution was also investigated. By varying the box size and resolution it is clear that the demands on resolution and computational box size grow with Grashof number as well as the time to reach a statistically steady state of fully developed turbulence. Using too a small computational domain in the spanwise direction results in a one-sided turbulent situation, which resembles the results of Ref. 9 where one-sided turbulence was obtained for the same computational box length in z as in the present study, but at higher Gr.

There is an increase of length scales due to buoyancy, which is evident from the correlation functions. The increase in the length scale of the turbulence decreases the dissipation of temperature fluctuations. This is pointed out as an explanation to why $\langle T'^2\rangle$ increases with Gr in the middle of the channel.

Periodicity in the time evolution of the wall shear stress is observed for high Grashof number. The period correlates fairly well to spatially extended internal gravity waves and thereby supports the hypothesis that the dominant structure is spatially extended internal gravity waves.

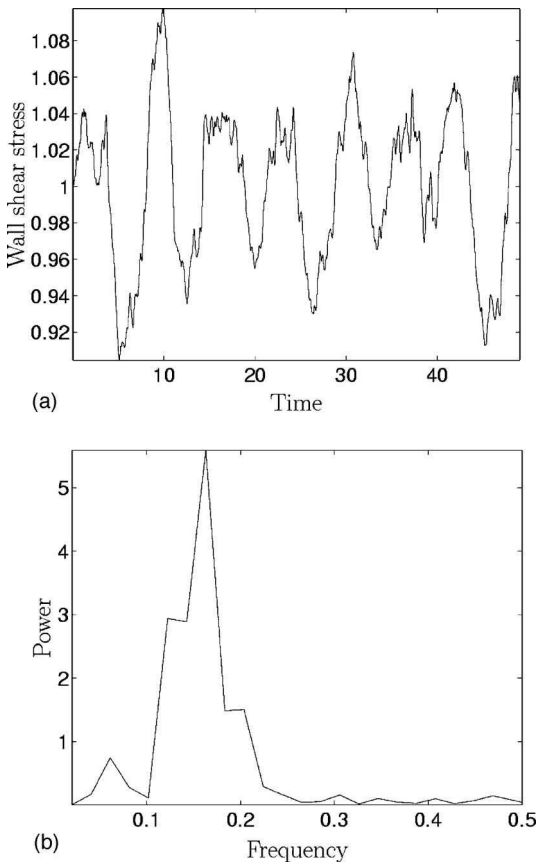

FIG. 8. Temporal evolution of the plane-averaged wall shear stress. The period time corresponding to max power spectra is 5.4. (a) Wall shear stress as function of time. Note the periodicity. (b) Power density spectra.

ACKNOWLEDGMENTS

The project in which this work was carried out is funded by VR (the Swedish National Research Board) and is a joint project between the Department of Electrodynamics and Department of Thermo and Fluid Dynamics at Chalmers University of Technology to study thermal instabilities and transport barriers in fluids and plasmas.

APPENDIX: BALANCES

The transport equations for $\langle k\rangle, \langle v^2\rangle, \langle T^2\rangle$, and $\langle vT\rangle$ are given below, where primed variables are defined as $f = f' + \langle f\rangle$

$$0 = \frac{\partial\langle k\rangle}{\partial t} = \mathrm{PT} + \mathrm{TT} + \mathrm{VT} + \mathrm{VD} + \mathrm{PR} + \mathrm{BU}, \tag{A1}$$

$$\mathrm{PT} = -\frac{\partial}{\partial y}\frac{\langle v' p'\rangle}{\rho} \text{ Pressure gradient velocity},$$

$$\mathrm{TT} = -\frac{\partial}{\partial y}\langle v' k\rangle \text{ Turbulent transport},$$

$$\mathrm{VT} = \frac{1}{\mathrm{Re}}\frac{\partial^2}{\partial y^2}\langle k\rangle \text{ Viscous transport},$$

$$\mathrm{VD} = -\frac{1}{\mathrm{Re}}\left\langle \frac{\partial u_j'}{\partial x_i}\frac{\partial u_j'}{\partial x_i}\right\rangle \text{ Viscous dissipation},$$

$$\mathrm{PR} = -\langle u' v'\rangle\frac{\partial\langle u\rangle}{\partial y} \text{ Turbulent production},$$

$$\mathrm{BU} = \frac{\mathrm{Gr}}{\mathrm{Re}^2}\langle v' T'\rangle \text{ Buoyancy term},$$

$$0 = \frac{\partial\langle v'^2\rangle}{\partial t} = \mathrm{TT} + \mathrm{PT} + \mathrm{BU} + \mathrm{VF}, \tag{A2}$$

$$\mathrm{TT} = -\left\langle \frac{\partial v'^3}{\partial y}\right\rangle \text{ Turbulent transport},$$

$$\mathrm{PT} = -2\left\langle v'\frac{\partial p'}{\partial y}\right\rangle \text{ Pressure gradient velocity},$$

$$\mathrm{BU} = 2\frac{\mathrm{Gr}}{\mathrm{Re}^2}\langle v' T'\rangle \text{ Buoyancy source},$$

$$\mathrm{VF} = \frac{1}{\mathrm{Re}}\frac{\partial^2\langle v'^2\rangle}{\partial y^2} \text{ Viscous diffusion},$$

$$\mathrm{VD} = -2\frac{1}{\mathrm{Re}}\left\langle \frac{\partial v'}{\partial x_j}\frac{\partial v'}{\partial x_j}\right\rangle \text{ Viscous dissipation},$$

$$0 = \frac{\partial\langle T'^2\rangle}{\partial t} = \mathrm{TT} + \mathrm{PTG} + \mathrm{VF}, \tag{A3}$$

$$\mathrm{TT} = -\frac{\partial}{\partial y}\langle T'^2 v'\rangle \text{ Turbulent transport},$$

$$\mathrm{PTG} = -2\langle v' T'\rangle\frac{\partial\langle T\rangle}{\partial y}$$

Production by temperature gradient,

$$\mathrm{VF} = \frac{1}{\mathrm{RePr}}\frac{\partial^2}{\partial y^2}\langle T'^2\rangle \text{ Viscous diffusion},$$

$$\mathrm{VD} = -2\frac{1}{\mathrm{RePr}}\left\langle \frac{\partial T'}{\partial x_j}\frac{\partial T'}{\partial x_j}\right\rangle \text{ Viscous dissipation},$$

$$0 = \frac{\partial\langle v' T'\rangle}{\partial t} = \mathrm{PTG} + \mathrm{TT} + \mathrm{PT} + \mathrm{VD} + \mathrm{VFV} + \mathrm{VFT} + \mathrm{BU}, \tag{A4}$$

$$\mathrm{PTG} = -\langle v'^2\rangle\frac{\partial}{\partial y}\langle T\rangle \text{ Production by temperature gradient},$$

$$\mathrm{TT} = -\frac{\partial}{\partial y}\langle v'^2 T'\rangle \text{ Turbulent transport},$$

$$\mathrm{PT} = -\left\langle T' \frac{\partial p'}{\partial y} \right\rangle \text{ Pressure gradient temperature},$$

$$\mathrm{VD} = -\left(\frac{1}{\mathrm{Re}} + \frac{1}{\mathrm{RePr}} \right) \left\langle \frac{\partial v'}{\partial x_j} \frac{\partial T'}{\partial x_j} \right\rangle \text{ Viscous dissipation},$$

$$\mathrm{VFV} = \frac{1}{\mathrm{Re}} \frac{\partial}{\partial y} \left\langle T' \frac{\partial v'}{\partial y} \right\rangle \text{ Diffusion by velocity gradients},$$

$$\mathrm{VFT} = \frac{1}{\mathrm{RePr}} \frac{\partial}{\partial y} \left\langle v' \frac{\partial T'}{\partial y} \right\rangle$$

Diffusion by temperature gradients,

$$\mathrm{BU} = \frac{\mathrm{Gr}}{\mathrm{Re}^2} \langle T'^2 \rangle \text{ Buoyant production}.$$

[1] P. Moin and K. Mahesh, "Direct numerical simulation: A tool in turbulence research," Annu. Rev. Fluid Mech. **30**, 539 (1998).
[2] E. J. Hopfinger, "Turbulence in stratified fluids: A review," J. Geophys. Res. **92**, 5287 (1987).
[3] B. A. Carreras, "Progress in anomalous transport research in toroidal magnetic confinement devices," IEEE Trans. Plasma Sci. **25**, 1281 (1997).
[4] R. Moestam, D. Sheikh, and J. Weiland, "A self consistent theory of zonal flows," Phys. Plasmas **11**, 4801 (2004).
[5] D. Lilly, "Stratified turbulence and mesoscal variability of the atmosphere," J. Atmos. Sci. **40**, 749 (1984).
[6] R. H. Kraichnan, "Internal ranges in two-dimensional turbulence," Phys. Fluids **10**, 1417 (1967).
[7] S. Komori, H. Ueda, F. Ogino, and T. Mizushina, "Turbulence structure in stably stratified open-channel flow," J. Fluid Mech. **130**, 13 (1983).
[8] C. Staquet and J. Sommeria, "Internal gravity waves: From instabilies to turbulence," Annu. Rev. Fluid Mech. **34**, 559 (2002).
[9] O. Iida, N. Kasagi, and Y. Nagano, "Direct numerical simulations of turbulent channel flow under stable density stratification," Int. J. Heat Mass Transfer **45**, 1693 (2002).
[10] P. Garg, J. Ferziger, S. Monismith, and J. Koseff, "Stably stratified turbulent channel flows. I. Stratification regimes and turbulence suppression mechanism," Phys. Fluids **12**, 2569 (2000).
[11] L. Davidson and S.-H. Peng, "Hybrid LES-RANS: A one-equation SGS model combined with a $k-\omega$ model for predicting recirculating flows," Int. J. Numer. Methods Fluids **43**, 1003 (2003).
[12] P. Emvin, "The full multigrid method applied to turbulent flow in ventilated enclosures using structured and unstructured grids," Ph.D. thesis, Department of Thermo and Fluid Dynamics, Chalmers University of Technology, Göthenburg, 1997.
[13] J. Pallares and L. Davidson, "Large-eddy simulations of turbulent flow in a rotating square duct," Phys. Fluids **12**, 2878 (2000).
[14] J. Pedlosky, *Geophysical Fluid Dynamics*, 2nd ed. (Springer, Berlin, 1992).
[15] R. Moestam, "Transport barriers in plasmas and fluids," Ph.D. thesis, ISBN 91-7291-328-2, Chalmers University of Technology, Department for Electromagnetics, 2003.